

[Click here to view linked References](#)

- 1 **Geomorphology and development of a high-latitude channel system: the INBIS Channel case (NW**  
2 **Barents Sea, Arctic).**  
3  
4  
5 3 Rui L.<sup>(1,7)</sup>, Rebesco M.<sup>(1)</sup>, Casamor J.L.<sup>(2)</sup>, Laberg J.S.<sup>(4)</sup>, Rydningen T.A.<sup>(4)</sup>, Caburlotto A.<sup>(1)</sup>, Forwick M.<sup>(4)</sup>,  
6  
7 4 Urgeles R.<sup>(3)</sup>, Accettella D.<sup>(1)</sup>, Lucchi R.G.<sup>(1)</sup>, Delbono I.<sup>(5)</sup>, Barsanti M.<sup>(5)</sup>, Demarte M.<sup>(6)</sup>, Ivaldi R.<sup>(6)</sup>.  
8  
9  
10 5 <sup>(1)</sup>OGS, Sgonico, TS, Italy;  
11  
12 6 <sup>(2)</sup>GRC Geociències Marines, Universitat de Barcelona, Spain;  
13  
14  
15 7 <sup>(3)</sup>Institut de Ciències del Mar, Consejo Superior de Investigaciones Científicas, Barcelona, Spain;  
16  
17  
18 8 <sup>(4)</sup>UiT The Arctic University of Norway in Tromsø, Department of Geosciences, Norway;  
19  
20  
21 9 <sup>(5)</sup>ENEA, Marine Environment Research Centre, La Spezia, Italy;  
22  
23  
24 10 <sup>(6)</sup>Italian Navy Hydrographic Institute, Genova, Italy;  
25  
26  
27 11 <sup>(7)</sup>University of Trieste, Trieste, Italy.  
28  
29  
30 12 **Keywords:** INBIS, channel system, Barents Sea, trough mouth fans, glaciated margin, <sup>210</sup>Pb dating method.  
31  
32  
33  
34  
35  
36  
37  
38  
39  
40  
41  
42  
43  
44  
45  
46  
47  
48  
49  
50  
51  
52  
53  
54  
55  
56  
57  
58  
59  
60  
61  
62  
63  
64  
65

## 13 Abstract

14 The INBIS (Interfan Bear Island and Storfjorden) Channel System is a rare example of a deep-sea channel on a  
15 glaciated margin. The system is located between two Trough Mouth Fans (TMFs) on the continental slope of the  
16 NW Barents Sea: the Bear Island and the Storfjorden-Kveithola TMFs. New bathymetric data in the upper part  
17 of this channel system shows a series of gullies that incise the shelf break and minor tributary channels on the  
18 upper part of the continental slope. These gullies and channels appears far more developed than those on the rest  
19 of the NW Barents Sea margin, increasing in size downslope and eventually merging into the INBIS Channel.  
20 Morphological evidence suggests that the Northern part of the INBIS Channel System preserved its original  
21 morphology over the Last Glacial Maximum (LGM), whereas the Southern part experienced the emplacement  
22 of mass-transport glacial debris that obliterated the original morphology. Radiometric analyses were applied  
23 on two sediment cores to estimate the recent (~ 110 years) sedimentation rates. Furthermore, analysis of grain  
24 size characteristics and sediment composition of two cores shows evidence of turbidity currents. We associate  
25 these turbidity currents with density-driven plumes, linked to the release of meltwater at the ice-sheet grounding  
26 line, cascading down the slope. This type of density current would contribute to the erosion and/ or preservation  
27 of the gullies' morphologies during the present interglacial. We infer that Bear Island and the shallow  
28 morphology around it prevented the flow of ice streams to the shelf edge in this area, working as a pin (fastener)  
29 for the surrounding ice and allowing for the development of the INBIS Channel System on the inter-ice stream  
30 part of the slope. The INBIS Channel System was protected from the burial by high rates of ice-stream derived  
31 sedimentation and only partially affected by the local emplacement of glacial debris, which instead dominated  
32 on the neighbouring TMF systems.

## 33 1. Introduction

34 Reconstruction of paleo-ice stream behaviour on a high-latitude glaciated continental margin is possible through  
35 the analysis of the associated characteristic features in the sedimentological and geomorphological record  
36 (*Stokes & Clark, 2001*). The most prominent features related to the activity of ice streams are the Trough Mouth  
37 Fans (TMFs). These are prograding fan-shaped sediment wedges are formed by glacial debris flows  
38 discharged by paleo-ice streams (*Vorren et al., 1989*). Gullies are small V-shaped erosional features that dissect  
39 the shelf edge and upper continental slope (*Noormets et al., 2009; Gales et al., 2013*). On high-latitude margins,  
40 potential gully-forming erosive mechanisms are: sediment-laden subglacial meltwater, discharged from the ice  
41 sheet, mainly during deglaciations (*Dowdeswell et al., 2006; Noormets et al., 2009; Lucchi et al., 2013; Llopart*

42 *et al., 2016; Zecchin et al., 2016*); dense bottom waters produced through sea-ice formation and brine rejection  
1  
2 43 (*Vorren et al., 1998*); turbidity currents (*Fohrmann et al., 1998*); iceberg scouring (*Dowdeswell & Bamber,*  
3  
4 44 *2007*); and glacigenic sediment flows (*Dowdeswell et al., 1998, 2002*). If the processes responsible for the  
5  
6 45 formation of gullies are persistent over time and/or increase in intensity, they can lead to the formation of  
7  
8 46 canyon-channel systems. These are larger net erosional to net depositional features that dissect the shelf edge  
9  
10 47 and extend across the seafloor from the continental shelf into the deep ocean (*Normark & Carlson, 2003;*  
11  
12 48 *Canals et al., 2004; Amblas et al., 2006, 2012; Harris & Whiteway, 2011*). The downslope part of these systems  
13  
14 49 can eventually evolve into U-shaped, lower-relief channels across the lower continental slope and beyond  
15  
16 50 (*Shepard & Emery, 1941; Normark et al., 1993*).

17  
18  
19 51 It is important to study underwater channel systems as they are the preferred route for the offshore transport of  
20  
21 52 sediment, nutrients and dense water masses. These systems are effectively carved by dense water and sediment-  
22  
23 53 gravity flows, delivering material from the shelf edge to the deep sea, particularly during sea-level low stand  
24  
25 54 periods (*Harris & Whiteway, 2011*). Therefore, the presence and the morphology of a channel system affect the  
26  
27 55 growth and the evolution of the continental margin and vice versa. On presently or formerly glaciated  
28  
29 56 continental margins the development of channel systems, aside from TMFs, is attributed to several mechanisms  
30  
31 57 related to the cycles of advances and retreats of past ice sheets. Therefore, the study of high-latitude channel  
32  
33 58 systems could lead to a better understanding of the dynamics of ice build-up and retreat and associated  
34  
35 59 glacigenic sediment transport during these periods. Moreover, the study of high-resolution data is essential to  
36  
37 60 increase our understanding on the spatial and temporal variability of glacimarine processes operating on high-  
38  
39 61 latitude margins (e.g. *Ó Cofaigh et al., 2013*). In fact, a marked lateral sedimentary variability of sedimentary  
40  
41 62 processes due to local physiography and hydrodynamics has been highlighted for this study area by *Zecchin et*  
42  
43 63 *al., 2018*.

44  
45  
46 64 The aim of this paper is to increase our understanding on the development of this part of the continental margin  
47  
48 65 during the late Quaternary. To achieve this aim we will; 1) study the morphology and the bathymetry of the  
49  
50 66 INBIS Channel System; 2) assess the role of down-slope and along-slope processes in the channel system  
51  
52 67 evolution; 3) identify the genetic mechanisms of the INBIS Channel System and its interactions with the nearby  
53  
54 68 TMF systems.

## 57 69 **2. Geological background and evolution of the Svalbard-Barents-Kara Ice Sheet (SBKIS)**

58  
59  
60  
61  
62  
63  
64  
65

70 Several studies have been conducted in order to reconstruct the timing and dynamics of the deglaciation of the  
71 NW Barents Sea and western Svalbard continental margins after the LGM (*Hyvärinen, 1968; Elverhøi et al.,*  
72 *1995; Salvigsen & Slettemark, 1995; Wohlfarth et al., 1995; Rasmussen et al., 2007; Jessen et al., 2010;*  
73 *Rebesco et al., 2011, 2014; Rütther et al., 2011*). Although the dynamics and exact timing of the deglaciation are  
74 still a matter of debate, there is agreement that the glacial retreat started in the deeper troughs due to the  
75 influence of ocean warming and sea-level rise (*Jones & Keigwin, 1988; Landvik et al., 1998; Winsborrow et al.,*  
76 *2010; Rütther et al., 2012*). The Last Glacial Maximum (LGM) in the area of the NW Barents Sea occurred  
77 around 23-19 ka, with the maximum ice extent reached at around 21.5 ka (*Patton et al., 2015*). At that time the  
78 Barents Sea Ice Sheet extended to the shelf edge of the western Barents Sea margin with areas of fast-flowing  
79 ice streams in the troughs and slower-flowing ice on the shallower banks (*Vorren & Laberg, 1996*). The onset of  
80 the deglaciation is inferred to have begun around 20-19 ka in the outermost part of west Spitsbergenbanken  
81 (*Elverhøi et al., 1995; Rasmussen et al., 2007*) and in the Kveithola Trough (*Pedrosa et al., 2011; Rebesco et*  
82 *al., 2011, 2016; Lucchi et al., 2013*). The deglaciation occurred as an alternation of rapid retreats, still stand  
83 periods and/or re-advances (*Rasmussen et al., 2007; Pedrosa et al., 2011; Rebesco et al., 2011, 2016;*  
84 *Bjarnadottir et al., 2013, 2017; Rütther et al., 2012*). In the Bear Island Trough, the ice stream started its retreat  
85 around 19.5 ka (*Patton et al., 2017*). However, it is inferred to have re-advanced hundreds of kilometres toward  
86 the shelf break at least three times before 17.8 ka (*Patton et al., 2017*) and at around 17.1 ka (*Rütther et al.,*  
87 *2011*) before starting its final, stepwise retreat (*Winsborrow et al., 2010; Andreassen et al., 2014, 2016*). In the  
88 final stages, the combination of abrupt sea-level rise and ocean warming triggered a retreat of 145 km in 700  
89 years, followed by the final decay of the ice stream by 13 ka (*Petrini et al., 2018*). The Bear Island (Bjørnøya),  
90 located between the Storfjorden and Bear Island Troughs, was ice-free at 11.2 cal. ka BP (*Wohlfarth et al.,*  
91 *1995*).

92 There are few systematic studies of channel systems on glaciated continental margins. A channel system on the  
93 East Greenland continental margin, in front of the Kaiser Franz Joseph Fjord, is inferred to be the oldest channel  
94 in the Norwegian – Greenland Sea (*Mienert et al., 1993; Dowdeswell et al., 2002; Ó Cofaigh et al., 2004;*  
95 *Wilken & Mienert, 2006; García et al., 2016; Peakall et al., 2012*). The start of the formation of this channel is  
96 dated to around 2.5 Ma (*Wilken & Mienert, 2006*). It originates at a water depth of about 1500 m on the  
97 continental slope, crosses glaciogenic debris flow deposits located on the lower part of the slope and extends  
98 north-east for 500 kilometres, terminating in the Greenland Basin at a water depth of 3700 m (*Wilken &*  
99 *Mienert, 2006*). The formation of this channel system is mainly attributed to sediment-laden meltwater produced

100 by the eastern Greenland Ice Sheet. Along the Norwegian and Svalbard continental margin, channel systems are  
1  
2 101 less developed compared to the East Greenland continental margin (*Wilken & Mienert, 2006*). So far, three large  
3  
4 102 deep-sea channel systems have been described: the Lofoten Basin Channel System (*Dowdeswell et al., 1996*;  
5  
6 103 *Vorren et al., 1998; Rise et al., 2013*), formed by the 30 km long Andøya Canyon and its continuation, a 300 km  
7  
8 104 long channel located in the SE Lofoten Basin, reaching a water depth of 3000 m (*Laberg et al., 2007; Amundsen*  
9  
10 105 *et al., 2015*); the Kongsfjorden Channel System (*Forwick et al., 2015*), a ~120 km long channel system located  
11  
12 106 on the continental slope off northwest Svalbard, between water depths of ~250-4000 m; and the INBIS Channel  
13  
14 107 System (*Vorren et al., 1998; Vorren & Laberg, 2001*) located on the continental slope west of Bear Island (NW  
15  
16 108 Barents Sea) (Fig. 1).

17  
18  
19 109 The INBIS Channel is a 60 km long and 5-15 km wide, nearly flat-bottomed east-west oriented channel, located  
20  
21 110 between water depths of ~2350 – 2520 m (Fig. 2). *Vorren et al. (1998)* attributes the formation of the INBIS  
22  
23 111 Channel to density-driven currents descending the southern flank of the Storfjorden TMF, the northern flank of  
24  
25 112 the Bear Island TMF and the inter-TMF area between these two TMFs. At that time, no bathymetry data were  
26  
27 113 available to show the large influence of the Kveithola TMF on the location of the INBIS Channel System. Core  
28  
29 114 analysis (GK 23257 in *Vorren et al., 1998*) suggests that these density-driven currents were active mainly during  
30  
31 115 glaciations. The origin of these density-driven currents is attributed to dense water formed by cooling under sea-  
32  
33 116 ice formation with brine rejection, or to turbidity currents generated from small landslides on the upper slope.  
34  
35 117 The INBIS Channel is partially infilled by glacial debris flows, which reached their main activity during  
36  
37 118 glacial maxima (*Vorren & Laberg, 1996; Vorren et al., 1998*).

### 39 40 119 **3 Data and Methods**

41  
42  
43 120 Data acquisition was carried out during four main oceanographic cruises: the EGLACOM (Evolution of a  
44  
45 121 GLacial Arctic COntinental Margin, July-August 2008) and the DEGLABAR (DEGLAciation History of the  
46  
47 122 North-Western BARents Sea from Sediments Generated by Paleo-Ice Streams Deglaciation history of the NW  
48  
49 123 BARents Sea, September 2015) cruises, both on board the Italian R/V OGS Explora; the CORIBAR (CORIng in  
50  
51 124 the NW BARents Sea, July-August 2013) cruise on board the German R/V Maria S. Merian; and the HN17  
52  
53 125 (High North 17, July 2017) cruise on board the NATO-MMI R/V Alliance. Swath bathymetry data were  
54  
55  
56 126 acquired during the main four cruises (see Table 1), and three box-cores were collected in the INBIS Channel  
57  
58 127 System area during HN17, providing indications of modern sedimentary environments in the study area. In  
59  
60  
61  
62  
63  
64  
65

128 addition, a minor part of Swath bathymetry data was acquired during the SVAIS (*Camerlenghi et al., 2007*) and  
129 GlaciBar (*Andreassen et al., 2009*) cruises.

### 130 **3.1 Swath bathymetry**

131 The swath bathymetry data collected during the EGLACOM and DEGLABAR cruises were acquired using  
132 Multibeam Echosounders (MBES) Reson MB8111 – MB8150 and Reson MB8111 – MB7150, respectively.  
133 During the CORIBAR cruise the swath bathymetry data was collected with Kongsberg EM1002 and EM 122  
134 MBES, whereas the MBES Kongsberg EM 302 was used during the HN17 cruise. All systems used were hull-  
135 mounted and had a swath of 150°.

136 The acquired data were processed using PDS2000 and CARIS. The processed data were merged into one dataset  
137 with a cell size of 30 m. During the last days of the DEGLABAR cruise, rough weather conditions affected the  
138 acquisition of bathymetric data, resulting in considerably lower data quality in the southernmost part of the  
139 INBIS Channel System.

### 140 **3.2 Ground truthing**

141 Ground truthing was performed at three sites using a box corer assembled with a box sized 30x20x50 cm,  
142 working with a 125 kg weighted head. The sediment box was sub-sampled with plastic liners for shore-based  
143 analyses. Each sediment core was logged visually (sediment colour code according to the Munsell Colour Chart)  
144 and by X-radiography. Physical properties were measured at 1-cm resolution with a multi-sensor core logger (P-  
145 wave velocity, wet bulk density, and loop sensor magnetic susceptibility). Qualitative element-geochemical  
146 measurements were performed with an Avaatech X-ray fluorescence (XRF) core scanner for light (10 kV) and  
147 heavy (30 kV) elements at 1-cm resolution. The results of the XRF core scanning are presented as calcium vs  
148 titanium ratio (Ca/Ti), giving indication of biological carbonate versus terrigenous sediment input (e.g.  
149 *Croudace et al., 2006*). Following *Wang et al. (2011)* and *Caricchi et al. (2018)*, the zirconium vs rubidium  
150 ratio (Zr/Rb) was used as a qualitative indicator of the grain size characteristics as Zr is usually contained in  
151 sand-sized sediment, whereas Rb is an element that is typically contained in clay minerals (c.f. *Wang et al.*  
152 *2011; Caricchi et al. 2018*).

### 153 **3.3 Radiometric analyses and dating model**

154 Sediment cores HN17-07BC2 and HN17-08BC3 (Fig. 4) were sliced at 1 cm resolution for Gamma ray  
155 spectrometry analyses carried out at ENEA Marine Environment Research Centre La Spezia (Italy), according  
156 to the methods described by *Delbono et al. (2016)*.  
157  $^{210}\text{Pb}_{\text{xs}}$  and  $^{137}\text{Cs}$  activities are measured in  $\text{Bq kg}^{-1}$  sediment dry weight.  $^{210}\text{Pb}$  dating method has been widely  
158 used for establishing geochronology in marine sediments, so that Sediment Accumulation Rate (SAR,  $\text{cm y}^{-1}$ )  
159 can be estimated, on time scales of  $\sim 110$  years, compatible with  $^{210}\text{Pb}$  physical half-life (*Appleby et al., 1979*;  
160 *Koide et al., 1972*; *Robbins et al., 1978*; *Sanchez-Cabeza and Ruiz-Fernández, 2012*). Among the typically used  
161 dating models based on  $^{210}\text{Pb}_{\text{xs}}$  profiles, in this paper we apply the *CRS model* that assumes a Constant Rate of  
162 Supply of  $^{210}\text{Pb}_{\text{xs}}$  (*Appleby and Oldfield, 1978*). The downcore  $^{137}\text{Cs}$  activity profiles are often used as an  
163 independent validation of  $^{210}\text{Pb}$  dating models (*Smith, 2001*), since they provide a similar clock with some well-  
164 defined temporal features such as the 1963 fallout peak (associated to nuclear bomb testing) and the 1986  
165 Chernobyl peak (*Carroll and Lerche, 2003*; *Robbins and Edgington, 1975*).

#### 166 **4 Results**

167 The studied area of the INBIS Channel System is divided into three morphological areas: 1) the upper reaches of  
168 the channel, 2) the northern and 3) southern sectors of the middle slope (Fig. 3).

##### 169 **4.1 The upper reaches of the INBIS Channel System**

170 The upper reaches of the INBIS Channel System have an amphitheatre shape extending from the Kveithola to  
171 the Bear Island TMFs (Fig. 2) for *ca.* 60 km. This gully-dominated part extends from the shelf edge, at a depth  
172 of *ca.* 420 m to a water depth ranging from 700 m in the north of the amphitheatre to 1100 m in the south.  
173 Further downslope the INBIS Channel System develops into a channel-dominated part. Along the upper reaches  
174 it is possible to identify 40 gullies with an average axial dip of  $4^\circ$  to  $5^\circ$ . The gullies are characterized by an  
175 overall V-shape (Fig. 5), with widths varying from 150 to 600 m, and incision depths varying from 10 to 60 m.  
176 The gullies originate at the shelf edge, with a lateral spacing of 450 m to 950 m in the northern area, increasing  
177 to approximately 2 km in the southern area (Fig. 3). The depth-to-width ratio of the incision is *ca.* 1/10. The  
178 bottom of the gullies is moderately smooth in the area close to the shelf break, with water depths varying  
179 between 420-750 m, becoming slightly rougher at water depths of *ca.* 800-900 m (Fig. 6, profile A). Levees are  
180 absent in the upper part of the INBIS Channel System.

181 On the shelf west of Bear Island, at a distance of 2 and 5 km from the shelf edge two curved ridges are present  
182 (Fig. 2). These ridges are about 2-3 km wide and a few tens of metres high, extending from the Kveithola  
183 Trough to the Bear Island Trough for ~100 km. These ridges are parallel and close to the shelf break in front of  
184 Bear Island, while more to the south they become more distant and more oblique with respect to the shelf break  
185 and subparallel to the Bear Island Trough flowlines.

#### 186 **4.2 The northern part of the middle slope**

187 The gradient of the middle slope in the northern part of the channel system is  $\sim 1^\circ$ - $2^\circ$  (Fig. 3). This area hosts 23  
188 of the 40 gullies present on the upper reaches. The gullies display symmetrical, V-shaped cross sections (Fig. 5),  
189 with a depth/width ratio of *ca.* 1/10, and variable sinuosity. The gullies converge downslope into larger  
190 channels, at water depths of 750-1000 m. At these depths, the channels are characterized by U-shaped cross  
191 profiles (Fig. 5) with widths varying between 600 and 2200 m, and incision depths of 30 to 150 m. Both incision  
192 depth and width increase downslope, while the thalweg of the channels become gradually rougher (Fig. 6). The  
193 ratio between incision depth and width decreases to around 1/20 with increasing water depth (Fig. 5). The inter-  
194 channel width is highly variable, ranging from hundreds of metres to a maximum of about 5 km (Fig. 3). Small  
195 levees were observed on the northern flank of some channels. The northernmost of these channels, which marks  
196 the northern limit of the INBIS channel system, has the shallowest incision depth (only a few metres), and its  
197 profile is highly asymmetric at a water depth of around 1200 m, with a lower gradient on the northern flank  
198 (Fig. 5). This channel merges downslope with three channels at a water depth of around 1600 m and eventually  
199 reaches the main channel (described further below) at a water depth of around 1820-1850 m (Fig. 3).

200 The other channels observed in the northern middle slope converge at water depth varying between 1250-1600  
201 m and eventually merge into one at a water depth of around 1600 m.

202 The main channel (resulting from the merging of the channels in both the northern and southern middle slopes)  
203 starts at a water depth of around 1800 m and its axis is E-W oriented. The shallower channel leading to it is  
204 about 1000 m wide until around 1850 m water depth (Fig. 3) where its width increases rapidly up to 2500 m and  
205 where its incision depth increases from 30 m to 150 m (Fig. 3). The surface of the thalweg is relatively flat in  
206 the shallower portions of the channel, and becomes increasingly rough in the deeper part (Fig. 6). The cross-  
207 channel profiles of the channel are relatively smooth and symmetric in the upper part, while they become  
208 progressively more asymmetric below 1150 m water depth, with a steeper gradient characterizing the northern  
209 side-wall. At about 1000 m and 1450 m water depth the northern side-wall of the channel is characterized by  $\sim 7$



210 meters high levees (Fig. 5, profiles D and F), whereas between water depths of 1200 and 1450 m the channel is  
211 bordered to the north by a slightly upward convex sedimentary body, with a variable vertical relief of 5-10  
212 metres and a width of about 4 km. The lower part of the Bear Island TMF (Fig. 2, 3) affects the orientation of  
213 the main channel around 1800 m water depth, forcing it into a WNW direction.

#### 214 **4.3 The southern part of the middle slope**

215 The southern part of the INBIS Channel System extends to a depth of about 1800 m (Fig. 3). The gradient of the  
216 slope is, in general, lower with respect to the northern area, with an average slope of about 1°. Here 17 of the  
217 gullies observed in the upper reaches converge. The southernmost 5 gullies continue beyond the data coverage,  
218 while the remaining 12 gullies merge into three U-shaped channels. The southern one is the most prominent,  
219 with a width ranging from 1150 to 2500 m and an incision depth of 40-60 m (Fig. 5, N). The other two channels  
220 are slightly smaller, and characterized by widths varying between 900-1100 m and incision depths ranging  
221 between 30 m and 50 m. These two channels partially braid between the water depths of 1450 m and 1700 m  
222 (Fig. 3).

#### 223 **4.4 Sedimentological characteristics and chronology of sub-surface sediments**

224 Core HN17-06BC1 recovered in the southern area of the INBIS Channel System, on the outer shelf close to the  
225 southernmost recognized gully (Fig. 3), recovered only a smear of terrigenous/detritic sand with pebbles and  
226 cobbles. A first attempt of coring at this site failed to recover any sediment. Hull-mounted Acoustic Doppler  
227 Current Profiler (ADCP) measurements of the local oceanographic configuration indicated the presence of  
228 northward flowing bottom currents on the outer shelf with a speed exceeding 40 cm/s (*Ivaldi et al., 2017*). The  
229 presence of a coarse grained, pebbly substrate combined with strong bottom currents prevented sediment  
230 sampling at this site.

231 Core HN17-07BC2, retrieved from the upper part of the slope (Fig. 3), contains about 6 cm of dark olive gray  
232 (Munsell 5y 3/2) fine to medium sand overlying very dark grey (Munsell 5y 3/1) layered silt (6–13 cm bsf) and  
233 silty-clay (13–15 cm bsf) sediments. The contact between the upper two lithological units is irregular, possibly  
234 erosive. The composition of the uppermost sand is mixed, with the terrigenous fraction mainly composed of  
235 rock fragments (detritic till) and the biogenic fraction composed of shelf derived, redeposited bioclasts. The  
236 relatively high Ca/Ti ratio and low magnetic susceptibility (Fig. 4) support the presence of bioclast-rich sands in  
237 the uppermost 6 cm overlying terrigenous sediments (low Ca/Ti ratio and high magnetic susceptibility). The

238  $^{210}\text{Pb}_{\text{xs}}$  profile in this core appears affected by mixing in the upper 5-6 cm bsf. as indicated by the relatively  
1  
2 239 constant  $^{210}\text{Pb}_{\text{xs}}$  profile with values around  $60 \pm 12 \text{ Bq kg}^{-1}$ , instead of a typical exponentially down-core  
3  
4 240 decreasing profile. Below 6-7 cm bsf to the core bottom, the mean  $^{210}\text{Pb}_{\text{xs}}$  activity is close to zero ( $4 \pm 3 \text{ Bq kg}^{-1}$ ),  
5  
6 241 although it never decays to zero value. Such a trend, coherent in both  $^{210}\text{Pb}_{\text{xs}}$  and  $^{137}\text{Cs}$  activity profiles,  
7  
8 242 indicates the presence of post-depositional processes acting on the whole sediment core (i.e. biological and/or  
9  
10 243 mechanical mixing such as anthropogenic fishing activity). Therefore, standard  $^{210}\text{Pb}_{\text{xs}}$  dating models are not  
11  
12 244 applicable for this core. However, the presence of  $^{210}\text{Pb}_{\text{xs}}$  through the whole core indicates sediment layers  
13  
14 245 younger than ~110 years.

16  
17 246 Core HN17-08BC3, recovered on the outer shelf, in the uppermost 4 cm contains coarse sand (Munsell 2.5y 3/2)  
18  
19 247 with scattered pebbles and cobbles overlaying a sharp, irregular base. Between 4–14 cm, there is a normally  
20  
21 248 graded interval formed at the base by faintly laminated sand to silt (Munsell 2.5y 4/3) and mottled clayey  
22  
23 249 sediments at the top (Munsell 5y 4/2). The normally graded unit overlays, with a sharp-irregular contact, deeper  
24  
25 250 fine grained mud sediments located at the base of the core (14–17 cm bsf, Munsell 5y 3/2). The composition of  
26  
27 251 the sands at the top is mainly terrigenous/detritic. The scarce biogenic fraction is mainly of shelf provenance  
28  
29 252 (e.g. bryozoa), with pristine shells of pteropods associated to pelagic deposition. The rest of the sedimentary  
30  
31 253 sequence is terrigenous as also indicated by the very low Ca/Ti ratio and higher magnetic susceptibility. The  
32  
33 254 normally graded interval described between 4-14 cm bsf can be also depicted by the trend of the Zr/Rb ratio  
34  
35 255 (Fig. 4). The  $^{210}\text{Pb}_{\text{xs}}$  activity profile in core HN17-08BC3 is characterized by a typical exponentially down-core  
36  
37 256 decrease with a well-defined  $^{210}\text{Pb}_{\text{xs}}$  zero value below 8-9 cm bsf. Applying the *CRS dating model*, the mean  
38  
39 257 value of Sediment Accumulation Rate (SAR) is  $0.06 \pm 0.02 \text{ cm y}^{-1}$ . In this core the  $^{137}\text{Cs}$  down-core profile  
40  
41 258 cannot be used as independent parameter to validate  $^{210}\text{Pb}$  dating profile, as  $^{137}\text{Cs}$  activities are too close to the  
42  
43 259 minimum detection limit and post-depositional processes cannot be ruled out. For this reason the above SAR  
44  
45 260 value should be considered as a maximum. Notwithstanding, the HN17-08BC3 SAR value is in agreement with  
46  
47 261 SAR values determined in the adjacent Kveithola TMF (*Caricchi et al. 2018*).

## 50 262 **5 Discussion**

### 53 263 **5.1 Morphology and depositional areas of the INBIS Channel System**

54  
55  
56 264 On the basis of the slope gradient we distinguished two main morphological areas in the INBIS Channel System  
57  
58 265 that, in turn, are characterized by different depositional processes: the upper reaches, which extends from the  
59  
60 266 shelf break to the upper continental slope, and the middle slope.

267 In the upper reaches, along the upper slope of the INBIS Channel System, the presence of predominantly V-  
1  
2 268 shaped gullies of similar size and regular spacing, with rarely developed levees, is associated with fast processes  
3  
4 269 of flow bypass and erosion responsible for down-slope sediment transport. The presence in the mid-slope  
5  
6 270 channel area of scarcely developed levees of small dimensions suggest that in this part of the INBIS Channel  
7  
8 271 System downslope sediment transport was restricted to the gullies' thalweg with occasional over spilling.  
9  
10 272 Bypass processes in the area might be related to the density-driven currents as the primary formation mechanism  
11  
12 273 of the INBIS Channel (e.g. *Vorren et al., 1998*). Such types of density-driven currents descending the southern  
13  
14 274 flank of the Storfjorden TMF, the northern flank of the Bear Island TMF and the inter-fan area in front of  
15  
16 275 Kveithola TMF were active mainly during glaciations. The origin of these density-driven currents has been  
17  
18 276 previously attributed to dense water formed by cooling and brine rejection during sea-ice formation and/or to  
19  
20 277 turbidity currents generated from small landslides on the upper slope (*Vorren et al., 1998; Forwick et al., 2015*).  
21  
22  
23 278 The gullies grow in dimension down the slope and develop into U-shaped channels (Fig. 5) with progressively  
24  
25 279 increasing rougher bases (Fig. 6). Gully growth might be related to intensification of erosion as a consequence  
26  
27 280 of the gullies/channels coalescence combined with a decrease in slope gradient. In the upper gully-dominated  
28  
29 281 part of the slope, the gradient is up to 5°, with consistent erosive processes determining V-shaped incisions.  
30  
31 282 Further downslope the gradient decreases down to 1° – 2 and the gullies evolve into wider, U-shaped channels.  
32  
33  
34 283 Similar V-shaped gullies on steep TMF slopes in both Arctic (e.g. *Rydningen et al., 2015*) and Antarctic (e.g.  
35  
36 284 *Noormets et al., 2009*) continental margins have been related to erosion by gravity-driven processes such as  
37  
38 285 high-energy, dense subglacial meltwaters occurring during deglaciation (e.g. *Lucchi et al., 2012, 2013; Gales et*  
39  
40 286 *al., 2013; Melis et al., 2018*).  
41  
42  
43 287 However, meltwaters are not the only flows that may have contributed to the formation of this upslope part of  
44  
45 288 the INBIS Channel System. During glacial maxima, sediments accumulate beyond the shelf edge, transported  
46  
47 289 and deposited by the ice streams. The collapse of these glacial sediment accumulations produces debris  
48  
49 290 flows (e.g. *Vorren et al., 1998; Laberg & Vorren, 1995, 1996, 2000;*). The INBIS Channel is marginally infilled  
50  
51 291 by glacial debris flows, which were most abundant during glacial maxima (*Laberg & Vorren, 1995*).  
52  
53  
54 292 We infer that the two curved ridges at 2 and 5 km from the shelf edge (Fig. 2) described in Section 4.1 are shelf-  
55  
56 293 edge moraines, subglacial landforms located in areas of slow-moving ice, similar to those observed west of the  
57  
58 294 Lofoten Islands on the western Norwegian margin (*Vorren et al., 2015; Batchelor and Dowdeswell, 2015;*  
59  
60 295 *Batchelor et al., 2017*). Another hypothesis is that these ridges are margin moraines formed in the transition  
61  
62  
63  
64  
65

296 zones between fast-flowing ice (ice streams) and slower-flowing ice (or absence of ice), similar to those  
1  
2 297 observed in the Vestfjorden Trough by *Ottesen et al. (2005)*.

3  
4  
5 298 In the middle slope of the INBIS Channel System, from about 1000 m water depth, the gullies merge into  
6  
7 299 channels. The flows originating the upper-slope gullies are funnelled through the centre of the area, and as a  
8  
9 300 consequence the larger channel forms. We infer that the merging of a large number of gullies into fewer  
10  
11 301 channels along with the gradient decrease may cause changes in the nature of the flows, causing irregular  
12  
13 302 erosion, similar to that observed in the Kongsfjorden Channel System by *Forwick et al. (2015)*. As a  
14  
15 303 consequence, in the deeper part of these channels the bottom roughness increases. Also the appearance of levees  
16  
17 304 suggests that the energy of the flows is sufficient to overtop the channels flanks.

18  
19  
20 305 Most of the other gullies/channels eventually converge downslope, and several processes probably led to the  
21  
22 306 asymmetry of the flanks here. First, due to the decreasing energy of the flows as a consequence of lower slope  
23  
24 307 gradient, the finest component of the sediment load is delayed and deflected to the right by the Coriolis force.  
25  
26 308 This produces overbank accumulations (levees) on the right (northern) flank of the main channel, similarly to  
27  
28 309 those reported for the lower INBIS Channel by *Vorren et al. (1998)*. Secondly, the northward-flowing West  
29  
30 310 Spitsbergen Current (WSC) may prevent sediments from settling on the southern side of the channels in this part  
31  
32 311 of the INBIS channel system, supporting deflection of the suspended sediment to the right of the channel and the  
33  
34 312 deposition of sediments on the northern side.

## 35 36 37 313 **5.2 Reconstruction of the geological history of the INBIS Channel System**

38  
39  
40 314 The morphogenetic analysis of the INBIS Channel System led to the identification of two main domains that  
41  
42 315 have undergone different geological evolution.

43  
44  
45 316 The *Northern area* (northern upper reaches and slope), characterized by sharp/pristine erosive structures, is the  
46  
47 317 area that possibly never experienced the arrival of massive, glacial debris flows. Such a type of morphology  
48  
49 318 can instead be compared with the canyon systems that typically dissect mid- and low-latitude margins (e.g.  
50  
51 319 Hudson Trough, *Mosher et al., 2017*) derived from river-incision on shelf sediments and erosion during low sea-  
52  
53 320 level stands, associated turbidity flows, and internal tide waves/currents. We believe the Northern area of the  
54  
55 321 INBIS Channel System developed through the funnelling of low-medium density flows, i.e.: turbidity currents  
56  
57 322 (*Fohrmann et al., 1998*) delivered during glacial times and early deglaciation; and plumes linked to the release  
58  
59 323 of meltwaters derived from basal glacial melting and retreat (*Dowdeswell et al., 2006; Noormets et al., 2009;*

324 *Lucchi et al., 2013; Llopart et al., 2016; Zecchin et al., 2016*); currents related to high salinity cold waters  
1  
2 325 (brine) originating from rejection during sea-ice formation (the latter process was already suggested by *Vorren*  
3  
4 326 *et al., 1998*). Furthermore, *Fohrmann et al. (1998)* indicated that consistent slope erosion presently occur by  
5  
6 327 means of mixed brine and suspended bottom sediments that generate powerful turbidity currents (so called *TS-*  
7  
8 328 *turbidites*). In support to this, we found evidence of turbidity currents and deposition in the studied upper slope  
9  
10 329 cores HN17-07BC2 (laminated sediments), and core HN17-08BC3 (normally graded deposits). In agreement  
11  
12 330 with the sedimentary facies described along the neighbouring Kveithola outer trough (*Lantzsch et al., 2017*), the  
13  
14 331 shelf edge of the INBIS Channel area appears presently swept by strong bottom currents (possibly the  
15  
16 332 northwards flowing West Spitsbergen Current). Such currents are responsible for deposition of the medium-  
17  
18 333 grained sands and pebbles lag deposit recovered at the top of cores HN17-07BC2 and HN17-08BC3, possibly  
19  
20 334 preventing sampling at site HN17-06BC1. This is supported also by the very low mean Sediment Accumulation  
21  
22 335 Rate ( $0.06 \pm 0.02 \text{ cm y}^{-1}$ ), calculated at station HN17-08BC3 for the last century.

23  
24  
25 336 Similar to the diversion of ice around topographic highs observed by *Knight et al., 2017* on the Greenland ice  
26  
27 337 sheet, we infer that the advances of the ice sheet, and in particular the ice streams in the studied area, were  
28  
29 338 partially diverted by the presence of Bear Island, preventing the formation of a continuum between the  
30  
31 339 Kveithola and the Bear Island TMFs. It is plausible that a local ice cap around Bear Island had already  
32  
33 340 developed before the surrounding ice streams reached the shelf break. We infer that when the SBKIS reached  
34  
35 341 this part of the margin, Bear Island worked as a pin (fastener) for the surrounding ice. The fast ice streams of  
36  
37 342 Bear Island and Kveithola diverged around Bear Island and flowed in the troughs (e.g. *Knies et al., 1999*;  
38  
39 343 *Dowdeswell et al., 2002; Rebesco et al, 2011, 2014; Lucchi et al., 2013*) (Fig. 7b), creating west of Bear Island  
40  
41 344 an inter-ice stream region of slower-flowing ice . We infer that the maximum extent of the local ice cap around  
42  
43 345 Bear Island is marked by the outermost of the ridges described in 4.1 (Fig. 2 and Fig. 7c).

44  
45  
46 346 The hypothesis that the SBKIS did not reach the shelf edge in this part of the margin is further supported by the  
47  
48 347 conceptual model of slope sedimentation on glacier-influenced continental margin of *Dowdeswell et al. (1998*;  
49  
50 348 *their Fig. 25; Dowdeswell et al., 1996; Pope et al., 2018)*. The elements constraining the model are the  
51  
52 349 proximity of the ice sheet/stream to the shelf edge, the sediment input and the type of sedimentary products. A  
53  
54 350 glacier-influenced margin is divided in three types: i) sediment starved margin, characterized by an ice sheet not  
55  
56 351 reaching the shelf edge, low sediment input and the formation of submarine channels; ii) inter-fan area,  
57  
58 352 characterized by an ice sheet reaching the shelf edge, moderate sediment input and the formation of mass  
59  
60  
61  
62  
63  
64  
65

353 transport deposits; iii) Trough Mouth Fan (TMF), characterized by an ice-stream reaching the shelf edge, the  
1  
2 354 highest sediment input and the formation of debris flow deposits. Although the INBIS Channel System is  
3  
4 355 located in an inter-fan area, where the inter-ice stream part of the ice sheet could potentially reach the shelf  
5  
6 356 edge, the slope is not characterized by landslide scars or landslide deposits, which are distinctive characteristics  
7  
8 357 of the slopes in inter-fan area on a glacier-influenced margin (e.g. *O'Grady et al., 2002; Pedrosa et al., 2011;*  
9  
10 358 *Madruzzani et al., 2018*). On the contrary, the formation of a submarine channel system is a characteristic of a  
11  
12 359 sediment starved margin, i.e. a part of the margin where the ice sheet did not reach the shelf edge (e.g. Kaiser  
13  
14 360 Franz Joseph Fjord, East Greenland, *Wilken & Mienert, 2006; Elverhøi et al., 1998*). We therefore infer that this  
15  
16 361 part of the continental margin is a special case of an inter-fan sediment starved area: the reduced amount of  
17  
18 362 sediment input is to be attributed to the slower-flowing ice not reaching the shelf edge due to the presence of  
19  
20 363 Bear Island. This hypothesis matches with the updated version of the model of glacier-influenced continental  
21  
22 364 margin presented by *Pope et al. (2018)*. In this schematic model, channel systems are expected to develop in  
23  
24 365 between glacial troughs in low sediment input margins (e.g. Fig. 28 in *Pope et al., 2018*). Another example of  
25  
26 366 channel formed in a sediment starved margin can be found on the continental slope north of Nordaustlandet  
27  
28 367 (Svalbard) in front of the Albertini Trough (*Fransner et al., 2018*). In this part of the margin there is large  
29  
30 368 accommodation space for sedimentation below the outer Albertini Trough due to down-faulted bedrock.  
31  
32 369 Therefore, the glacial sediments transported by ice streaming through the Albertini Trough accumulated in  
33  
34 370 the accommodation space of the outer-shelf basin, preventing the formation of a TMF and allowing the  
35  
36 371 formation of a submarine channel (*Fransner et al., 2018*).  
37  
38  
39 372 The *Southern area* (southern upper reaches and slope) is characterized by smoothed erosive structures that,  
40  
41 373 according to the morphological analysis, suggest the presence of relict mass transport deposits crossing the  
42  
43 374 upper slope with a SE-NW orientation (Fig. 7b, 7c). We argue that these mass transport deposits did not  
44  
45 375 originate on the slope as submarine landslides and they might actually represent glacial debris flows  
46  
47 376 delivered to the southern INBIS Channel System area by the northern fringe of the Bear Island ice stream during  
48  
49 377 past glacial maxima. The morphological evidences supporting this hypothesis include: a remarkably lower  
50  
51 378 gradient of the upper slope (about 1° versus up to 5° of the Northern area) that is comparable to the  
52  
53 379 neighbouring TMF, with deeper location of the gradient change between the upper and middle slope (1100 m  
54  
55 380 water depth instead than 700 m water depth in the Northern area); the reduced incision depth of the gullies (10  
56  
57 381 m depth) with respect to the northern area (60 m depth); a reduced number of secondary channels on the middle  
58  
59 382 slope that are characterized by a relatively small height/width ratio (1/20 instead of 1/10 of the Northern area).  
60  
61  
62  
63  
64  
65

383 According to the morphologies observed on the INBIS channel and surrounding areas we infer that such  
1  
2 384 glacial debris flows must have been emplaced on the slope earlier than the Middle Weichselian glaciation.  
3  
4 385 We argue that the southern channels might have been carved on high-density glacial debris flows, resulting  
5  
6 386 in a less pronounced shape than the channels observed in the Northern area of the INBIS Channel System.  
7  
8 387 Nevertheless, the channels are clearly marked on the sea floor, whereas on the neighbouring TMF systems, that  
9  
10 388 received glacial debris flows during LGM, the gullies of the upper slope never developed as proper channels  
11  
12 389 after the LGM (see *Pedrosa et al., 2011*).

13  
14  
15 390 Similar glacial dynamics were possibly responsible for the emplacement of the glacial debris flows observed on  
16  
17 391 the middle slope of the Northern area of the INBIS Channel System. We infer that glacial debris flows from  
18  
19 392 the Kveithola Trough never reached the upper reaches of the INBIS Channel System (presence of sharp pristine  
20  
21 393 morphologies), but they only partially invaded the middle slope, burying some of the former channels that  
22  
23 394 appear less pronounced or almost completely obliterated, as seen on the bathymetry (Fig. 3, 7c).

24  
25  
26 395 Beside of the relatively recent glacial history of the margin attaining to the present INBIS Channel system,  
27  
28 396 another hypothesis could explain the formation of a channel system in this inter-TMF area. As a matter of fact,  
29  
30 397 we cannot exclude the possibility that the initial onset of this channel system pre-dates the beginning of glacial  
31  
32 398 conditions. This system could in fact have been the deeper extension of a river system associated with the main  
33  
34 399 sub-aerial relief of Bear Island. The presence of an east-west oriented system of rivers transporting sediments to  
35  
36 400 the margin of the NW Barents Sea has been previously envisaged for the period preceding about 2 Ma by  
37  
38 401 *Hjelstuen et al (1996)*.

## 41 402 **6 Conclusions**

42  
43  
44 403 In this paper, we presented a morphological description of the upper slope area of the INBIS Channel System  
45  
46 404 based on newly acquired bathymetric data. We discussed its genesis and evolution during glacial maxima as  
47  
48 405 well as at present time, its interactions with the TMF systems and its role in sediment drainage to the deeper  
49  
50 406 environment on the west Spitsbergen margin.

- 51  
52  
53 407 • We identified 40 V-shaped gullies dissecting the shelf edge that increase in size downslope, merging  
54  
55 408 with adjacent gullies and evolving into larger U-shaped secondary channels. Secondary channels merge  
56  
57 409 down slope into the main INBIS Channel due to lateral confinement by the fringes of the Kveithola and  
58  
59 410 Bear Island TMFs.

- 411 • Two morphodynamic areas were distinguished within the INBIS Channel System characterized by  
 1 different geological evolution and drainage system: the Northern area representing a special case of  
 2 412 inter-fan, sediment starving margin, and the Southern areas with a more typically inter-fan related  
 3 sedimentation.  
 4 413  
 5 414  
 6  
 7  
 8  
 9 415 • The shelf break of the Northern area never experienced the massive arrival of glacial debris,  
 10 preserving its original morphologies over the past glaciations. Only the middle slope was affected by  
 11 416 the emplacement of glacial debris flows as part of the Kveithola TMF.  
 12 417  
 13  
 14  
 15  
 16 418 • The peculiarity of the continental margin attaining to the INBIS Channel System was attributed to the  
 17 formation, during the past glaciations, of slower-flowing ice associated to the presence of the Bear  
 18 419 Island that acts as a pin for the surrounding ice.  
 19 420  
 20  
 21  
 22  
 23 421 • After the onset of glaciations, the system was maintained through time by meltwater release during the  
 24 ice sheet retreat/decay, and by the erosive effect of brine and other dense gravity currents presently  
 25 422 forming on the shelf (TS turbidites) as recorded in sub-surface sediment cores.  
 26 423  
 27  
 28  
 29

## 30 424 **7 Acknowledgements**

31  
 32  
 33 425 This research was supported by the Italian projects PNRA-EDIPO, the project PNRA-CORIBAR, the rewarding  
 34 426 funding project ARCA and the project High North 17, and Spanish projects DEGLABAR (CTM2010-17386)  
 35 427 and CORIBAR-ES (CTM2011-14807-E), funded by the Spanish *Ministerio de Economía y Competitividad* and  
 36 428 the European Regional Development Fund.  
 37  
 38  
 39  
 40  
 41

42 429 **On behalf of all authors, the corresponding author states that there are no conflicts of interest.**

## 43 44 45 430 **8 References**

- 46  
 47  
 48 431 Amblas D., Canals M., Urgeles R., Lastras G., Liqueste C., Hughes-Clarke J.E., Casamor J.L., Calafat A.M.,  
 49 432 2006, *Morphogenetic mesoscale analysis of the northeastern Iberian margin, NW Mediterranean Basin*, *Marine*  
 50 433 *Geology* 234, pp. 3–20.  
 51  
 52  
 53  
 54 434 Amblas D., Gerber T.P., De Mol B., Urgeles R., Garcia-Castellanos D., Canals, M., Pratson L.F., Robb N.,  
 55 435 Canning J., 2012, *Survival of a submarine canyon during long-term outbuilding of a continental margin*,  
 56 436 *Geology* 40, pp. 543–546.  
 57  
 58  
 59  
 60  
 61  
 62  
 63  
 64  
 65



- 437 Amundsen H.B., Laberg J.S., Vorren T.O., Haflidason H., Forwick M., Buhl-Mortensen P., 2015, *Late*  
1  
2 438 *Weichselian – Holocene evolution of the high-latitude Andøya submarine canyon, North-Norwegian continental*  
3  
4 439 *margin*, Marine Geology 363, pp. 1-14.  
5  
6  
7 440 Andreassen K., Winsborrow M., Bjarnadóttir L., Rütther D., Borque J., Lucchi R., Caburlotto A., 2009, *Barents*  
8  
9 441 *Sea and the West Spitsbergen Margin, UiT 2009. Marine Geophysical/Geological Cruise to Outer Bear Island*  
10  
11 442 *trough, Kveithola trough and the West Spitsbergen Margin*, Cruise Report. RV/Jan Mayen 2.-19.07.2009  
12  
13 443 University of Tromsø, p. 33.  
14  
15  
16 444 Andreassen K., Winsborrow M.C.M., Bjarnadóttir L.R., Rütther D.C., 2014, *Ice stream retreat dynamics*  
17  
18 445 *inferred from an assemblage of landforms in the northern Barents Sea*, Quat. Sci. Rev.  
19  
20  
21 446 Andreassen K., Bjarnadóttir L.R., Rütther D.C., Winsborrow M.C.M., 2016, *Retreat patterns and dynamics of*  
22  
23 447 *the former Bear Island Trough Ice Stream*, Geological Society, London, Memoirs, 46, pp. 445-452.  
24  
25  
26 448 Appleby P.G., Oldfield F., 1978, *The calculation of lead-210 dates assuming a constant rate of supply of*  
27  
28 449 *unsupported 210Pb to the sediment*. Catena 5, pp. 1–8.  
29  
30  
31 450 Appleby P.G., 1979, *210Pb dating of annually laminated lake sediment from Finland*. Nature, 280, pp. 53-55.  
32  
33  
34 451 Batchelor C.L., Dowdeswell J.A., 2015, *Ice-sheet grounding-zone wedges (GZWs) on high-latitude continental*  
35  
36 452 *margins*, Marine Geology 363, pp. 65-92.  
37  
38  
39 453 Batchelor C.L., Dowdeswell J.A., Ottensen D., 2017, *Submarine Glacial Landforms*, in: Micallef A., Krastel S.,  
40  
41 454 Savini A., 2017, *Submarine Geomorphology*, pp. 207 – 234.  
42  
43  
44 455 Bjarnadóttir L.R., Rütther D.C., Winsborrow M.C.M., Andreassen K., 2013, *Grounding-line dynamics during*  
45  
46 456 *the last deglaciation of Kveithola, W Barents Sea, as revealed by seabed geomorphology and shallow seismic*  
47  
48 457 *stratigraphy*, Boreas, 42, pp. 84-107  
49  
50  
51 458 Bjarnadóttir L.R., Winsborrow M.C.M., Andreassen K., 2017, *Large subglacial meltwater features in the*  
52  
53 459 *central Barents Sea*, Geology, 45, pp. 159–162.  
54  
55  
56 460 Camerlenghi A., Flores J.A., Sierro F.J., Colmenreo E., the SVAIS Scientific and Technical Staff, 2007, *SVAIS,*  
57  
58 461 *the Development of an Ice Stream-dominated Sedimentary System: the Southern Svalbard Continental Margin,*  
59  
60 462 *Cruise report*, University of Barcelona, p. 62.  
61  
62  
63  
64  
65

- 463 Canals M., Casamor J.L., Lastras G., Monaco A., Acosta Y.J., Berne S., Loubrieu B., Weaver P., Greham A.,  
1  
2 464 Dennielou B., 2004, *The Role of Canyons in Strata Formation*, Oceanography (Washington D.C.) 17, pp. 80-91.  
3  
4  
5 465 Caricchi C., Lucchi R.G., Sagnotti L., Macrì P., Morigi C., Melis R., Caffau M., Rebesco M., Hanebuth T.J.J.,  
6  
7 466 2018, *Paleomagnetism and rock magnetism from sediments along a continental shelf-to-slope transect in the*  
8  
9 467 *NW Barents Sea: Implications for geomagnetic and depositional changes during the past 15 thousand years*,  
10  
11 468 *Global and Planetary Change* 160, pp. 10-27.  
12  
13  
14 469 Carroll J., Lerche I., 2003. *Sedimentary Processes: Quantification Using Radionuclides*. Elsevier, Oxford.  
15  
16  
17 470 Croudace I.W., Rindby A., Guy Rothwell R.G., 2006, *ITRAX: description and evaluation of a new multi-*  
18  
19 471 *function X-ray core scanner*, Geological Society, London, Special Publications, 267, pp. 51-63.  
20  
21  
22 472 Delbono I., Barsanti M., Schirone A., Conte F., Delfanti R., 2016. *210Pb mass accumulation rates in the*  
23  
24 473 *depositional area of the Magra River (Mediterranean Sea, Italy)*. *Cont. Shelf Res.* 124, pp. 35–48.  
25  
26  
27 474 Dowdeswell J.A., Kenyon N., Elverhoi A., Laberg J.S., Mienert J., Siegert M.J., 1996, *Large-scale*  
28  
29 475 *sedimentation on the glacier-influenced Polar North Atlantic margins: long range side-scan sonar evidence*,  
30  
31 476 *Geophysical, Research Letters*, 23, pp. 3535-3538.  
32  
33  
34 477 Dowdeswell J.A., Elverhøi A., Spielhagen R., 1998, *Glacimarine sedimentary processes and facies on the Polar*  
35  
36 478 *North Atlantic Margins*, *Quaternary Science Reviews*, vol. 17, pp. 243-272.  
37  
38  
39 479 Dowdeswell J.A., Ó Cofaigh C., Taylor J., Kenyon N.H., Mienert J., Wilken M., 2002, *On the architecture of*  
40  
41 480 *high-latitude continental margins: the influence of ice-sheet and sea-ice processes in the Polar North Atlantic*,  
42  
43 481 *In: Dowdeswell, J.A. & Ó Cofaigh C., 2002, Glacier-Influenced Sedimentation on High-Latitude Continental*  
44  
45 482 *Margins*, Geological Society, London, Special Publications 203, pp. 33-54.  
46  
47  
48 483 Dowdeswell J.A., Evans J., Cofaigh C. Ó., Anderson J.B., 2006, *Morphology and sedimentary processes on the*  
49  
50 484 *continental slope of Pine Island Bay, Amundsen Sea, West Antarctic*, *Geological Society of America Bulletin*  
51  
52 485 118 (5/6), pp. 606–619.  
53  
54  
55 486 Dowdeswell J.A., Bamber J.L., 2007, *Keel depths of modern Antarctic icebergs and implications for sea-floor*  
56  
57 487 *scouring in the geological record*, *Marine Geology* 243, pp. 120–131.  
58  
59  
60  
61  
62  
63  
64  
65

- 488 Elverhøi A., Andersen E.S., Dokken T., Hebbeln D., Spielhagen R., Svendsen J.I., Sorflaten M., Rornes A.,  
1  
2 489 Hald M., Forsberg C.F., 1995, *The growth and decay of the late Weichselian ice sheet in western Svalbard and*  
3  
4 490 *adjacent areas based on provenance studies of marine sediments*, Quat. Res. 44, pp. 303-316.  
5  
6  
7 491 Elverhøi A., Dowdeswell J.A., Funder S., Mangerud J., Stein R., 1998, *Glacial and oceanic history of the polar*  
8  
9 492 *north Atlantic margins: an overview*, Quaternary Science Reviews 17, pp. 1-10.  
10  
11  
12 493 Fohrmann H., Backhaus J.O., Blaume F., Rumohr J., 1998, *Sediments in bottom-arrested gravity plumes:*  
13  
14 494 *Numerical case studies*, J. Phys. Oceanogr. 28, pp. 2250-2274.  
15  
16  
17 495 Forwick M., Laberg J.S., Hass H.C., Osti G., 2015, *The Kongsfjorden Channel System offshore NW Svalbard:*  
18  
19 496 *downslope sedimentary processes in a contour-current-dominated setting*, Arktos, 1 (1).  
20  
21  
22 497 Fransner O., Noormets R., Flink A.E., Hogan K.A., Dowdeswell J.A., 2018, *Sedimentary processes on the*  
23  
24 498 *continental slope off Kvitøya and Albertini troughs north of Nordaustlandet, Svalbard – The importance of*  
25  
26 499 *structural-geological setting in trough-mouth fan development*, Marine Geology 402, pp 194-208.  
27  
28  
29 500 Gales J.A., Forwick M., Laberg J.S., Vorren T.O., Larter R.D., Graham A.G.C., Baeten N.J., Amundsen H.B.,  
30  
31 501 2013, *Arctic and Antarctic submarine gullies – A comparison of high latitude continental margins*,  
32  
33 502 *Geomorphology* 201, pp. 449-461.  
34  
35  
36 503 García M., Batchelor C.L., Dowdeswell J.A., Hogan K.A., Cofaigh Ó., 2016, *A glacier-influenced turbidite*  
37  
38 504 *system and associated landform assemblage in the Greenland Basin and adjacent continental slope*, In:  
39  
40 505 Dowdeswell J.A., Canals M., Jackobbson M., Todd B.J., Dowdeswell E.K., Hogan K.A., 2016, *Atlas of*  
41  
42 506 *Submarine Glacial Landforms: Modern, Quaternary and Ancient*, Geological Society, London, Memoirs, 46,  
43  
44 507 pp. 461-468.  
45  
46  
47 508 Harris P.T., Whiteway T., 2011, *Global distribution of large submarine canyons: geomorphic differences*  
48  
49 509 *between active and passive continental margins*, Marine Geology 285, pp. 69–86.  
50  
51  
52 510 Hjelstuen B.O., Elverhøi A., Faleide J.I., 1996, *Cenozoic erosion and sediment yield in the drainage area of the*  
53  
54 511 *Storfjorden Fan*, Global Planet. Change, 12, pp. 95-117.  
55  
56  
57 512 Hughes A. L. C., Gyllencreutz R., Lohne Ø. S., Mangerud J., Svendsen J. I., 2016, *The last Eurasian ice sheets*  
58  
59 513 *– a chronological database and time-slice reconstruction, DATED-1*, Boreas, Vol. 45, pp. 1–45.  
60  
61  
62  
63  
64  
65

- 1  
2  
3  
4  
5  
6  
7  
8  
9  
10  
11  
12  
13  
14  
15  
16  
17  
18  
19  
20  
21  
22  
23  
24  
25  
26  
27  
28  
29  
30  
31  
32  
33  
34  
35  
36  
37  
38  
39  
40  
41  
42  
43  
44  
45  
46  
47  
48  
49  
50  
51  
52  
53  
54  
55  
56  
57  
58  
59  
60  
61  
62  
63  
64  
65
- 514 Hyvärinen H. 1968, *Late-Quaternary sediment cores from lakes on Bjørnøya*, Geografiska Annaler 50, pp. 235–  
515 245.
- 516 Ivaldi R., Demarte M. and HIGH NORTH 17 Team, 2017, *HIGH NORTH 17 cruise report*, Istituto Idrografico  
517 della Marina, pp. 1-70.
- 518 Jakobsson M., et al., 2012, *The International Bathymetric Chart of the Arctic Ocean (IBCAO) Version 3.0*,  
519 Geophys. Res. Lett., 39.
- 520 Jessen S.P., Rasmussen T.L., Nielsen T., Solheim A., 2010, *A new Late Weichselian and Holocene marine*  
521 *chronology for the western Svalbard slope 30,000-0 cal years BP*, Quaternary Science Reviews 29, pp. 1301-  
522 1312.
- 523 Jones G.A., Keigwin, L.D., 1988, *Age determinations on sediment core PS1295-4*, Supplement to: Jones G.A.,  
524 Keigwin L.D., 1988, *Evidence from Fram Strait (78°N) for early deglaciation*, Nature, 336(6194), pp. 56-59.
- 525 Knies J., Vogt C., Stein R., 1999, *Late Quaternary growth and decay of the Svalbard/Barents Sea ice sheet and*  
526 *paleoceanographic evolution in the adjacent Arctic Ocean*, Geo-Marine Letters, 18, pp. 195-202.
- 527 Knight P., Sugden D., Minty C., 1994, *Ice flow around large obstacles as indicated by basal ice exposed at the*  
528 *margin of the Greenland ice sheet*, Journal of Glaciology, 40(135), pp. 359-367.
- 529 Koide M., Soutar A., Goldberg E.D., 1972. *Marine geochronology with 210Pb*. Earth Planet. Sci. Lett. 14, pp.  
530 442–446.
- 531 Laberg J.S., Vorren T.O., 1995, *Late Weichselian submarine debris flow deposits on the Bear Island Trough*  
532 *Mouth Fan*, Mar. Geol., 127 (1–4), pp. 45-72.
- 533 Laberg J.S., Vorren T.O., 1996, *The Middle and Late Pleistocene evolution of the Bear Island Trough Mouth*  
534 *Fan*, Global and Planetary Change 12, pp. 309-330.
- 535 Laberg J.S., Vorren T.O., 2000, *Flow behaviour of the submarine glacial debris flows on the Bear Island*  
536 *Trough Mouth Fan, western Barents Sea*, Sedimentology 47, pp. 1105-1117.
- 537 Laberg J.S., Guidard S., Mienert J., Vorren T.O., Haflidason H., Nygård A., 2007, *Morphology and*  
538 *morphogenesis of a high-latitude canyon; the Andøya Canyon, Norwegian Sea*, Marine Geology 246, pp. 68-85.

- 539 Landvik J.Y., Bondevik S., Elverhøi A., Fjeldskaar W., Mangerud J., Salvigsen O., Siegert M.J., Svendsen J.I.,  
1  
2 540 Vorren T.O., 1998, *The last glacial maximum of Svalbard and the Barents Sea area: ice sheet extent and*  
3  
4 541 *configuration*, Quat. Sci. Rev. 17, pp. 43–75.  
5  
6  
7 542 Lantzsch H., Hanebuth T.J.J., Horry J., Grave M., Rebesco M., Schwenk T., 2017, *Deglacial to Holocene*  
8  
9 543 *history of ice-sheet retreat and bottom current strength on the western Barents Sea shelf*, Quaternary Science  
10  
11 544 Reviews 173, pp. 40-57.  
12  
13  
14 545 Llopart J., Urgeles R., Camerlenghi A., Lucchi R.G., De Mol B., Rebesco M., Pedrosa M.T., 2016, *Slope*  
15  
16 546 *instability of glaciated continental margins: Constraints from permeability-compressibility tests and*  
17  
18 547 *hydrogeological modelling off Storfjorden, NW Barents Sea*, Submarine Mass Movements and Their  
19  
20 548 Consequences, 6th International Symposium, pp. 95-104.  
21  
22  
23 549 Lucchi R.G., Pedrosa M.T., Camerlenghi A., Urgeles R., De Mol B., Rebesco M., 2012, *Recent submarine*  
24  
25 550 *landslides on the continental slope of Storfjorden and Kveithola Trough-Mouth Fans (north west Barents Sea)*,  
26  
27 551 In: Yamada Y., Kawamura K., Ikehara K., Ogawa Y., Urgeles R., Mosher D., Chaytor J., Strasser M. (Eds.),  
28  
29 552 *Submarine Mass Movements and Their Consequences. Advances in Natural and Technological Hazards*  
30  
31 553 *Research*, Springer Science book series, 31, pp. 735–745.  
32  
33  
34 554 Lucchi R.G., Camerlenghi A., Rebesco M., Urgeles R., Sagnotti L., Macri P., Colmenero- Hildago E., Sierro  
35  
36 555 F.J., Melis R., Morigi C., Barcena M.A., Giorgetti G., Villa G., Persico D., Flores J.A., Pedrosa M.T.,  
37  
38 556 Caburlotto A., 2013, *Postglacial sedimentary processes on the Storfjorden and Kveithola trough-mouth fans:*  
39  
40 557 *impact of extreme glacimarine sedimentation*, Glob. Planet. Change 111, pp. 309-326.  
41  
42  
43 558 Madrussani G., Rossi G., Rebesco M., Picotti S., Urgeles R., Llopart J., 2018, *Sediment properties in submarine*  
44  
45 559 *mass-transport deposits using seismic and rock-physics off NW Barents Sea*, Marine Geology 402, pp. 264-278.  
46  
47  
48 560 Melis R., Carbonara K., Villa G., Morigi C., Barcena M.A., Giorgetti G., Caburlotto A., Rebesco M., Lucchi  
49  
50 561 R.G., 2018, *A new multi-proxy investigation of Late Quaternary palaeoenvironments along the north-western*  
51  
52 562 *Barents Sea (Storfjorden Trough Mouth Fan)*, Journal of Quaternary Science 33, pp. 662-676.  
53  
54  
55 563 Mienert J., Kenyon N.H., Thiede J., Holender F.-J., 1993, *Polar continental margins: studies off East*  
56  
57 564 *Greenland*, EOS, Transactions of the American Geophysical Union 74, pp. 225-236.  
58  
59  
60  
61  
62  
63  
64  
65

- 565 Mosher D.C., Campbell D.C., Gardner J.V., Piper D.J.W., Chaytor J.D., Rebesco M., 2017, *The role of deep-*  
1 *water sedimentary processes in shaping a continental margin: The Northwest Atlantic*, Marine Geology 393, pp.  
2 245-259.  
3  
4  
5  
6  
7 568 Noormets R., Dowdeswell J.A., Larter R.D., Cofaigh C.Ó., Evans J., 2009, *Morphology of the upper continental*  
8 *slope in the Bellingshausen and Amundsen Seas – Implications for sedimentary processes at the shelf edge of*  
9 *West Antarctica*, Marine Geology 258, pp. 100-114.  
10  
11  
12  
13  
14 571 Normark W.R., Posamentier H., Mutti E., 1993, *Turbidite systems: State of the art and future*  
15 *directions*, Reviews of Geophysics, v. 31, pp. 91–116.  
16  
17  
18  
19 573 Normark W.R., Carlson P.R., 2003, *Giant submarine canyons: Is size any clue to their importance in the rock*  
20 *record?*, in: Extreme depositional environments: mega end members in geologic time, Geological Society of  
21 America, Vol. 370.  
22  
23  
24  
25 576 Ò Cofaigh C., Dowdeswell J.A., et al. 2004, *Timing and significance of glacially influenced mass-wasting in the*  
26 *submarine channels of the Greenland Basin*, Marine Geology 207, pp. 39-54.  
27  
28  
29  
30 578 Ò Cofaigh C., Andrews J.T., Jennings A.E., Dowdeswell J.A., Hogan K.A., Kilfeather A.A., Sheldon C., 2013,  
31 *Glacimarine lithofacies, provenance and depositional processes on a West Greenland trough-mouth fan*,  
32 *Journal of Quaternary Science*, pp. 13-26.  
33  
34  
35  
36  
37 581 O’Grady D.B., Syvitsky J.P.M., 2002, *Large-scale morphology of Arctic continental slopes: the influence of*  
38 *sediment delivery on slope form*, Geological Society, London, Special Publications 203, pp. 11-31.  
39  
40  
41  
42 583 Ottesen D., Rise L., Knies J., Olsen L., Henriksen S., 2005, *The Vestfjorden-Trænadjupet palaeo-ice stream*  
43 *drainage system, mid-Norwegian continental shelf*, Marine Geology 218, pp. 175-189.  
44  
45  
46  
47 585 Patton H., Andreassen K., Bjarnadóttir L.R., Dowdeswell J.A., Winsborrow C.M., Noormets R., Polyak L.,  
48 Auriac A., Hubbard A., 2015, *Geophysical constraints on the dynamics and retreat of the Barents Sea Ice Sheet*  
49 *as a palaeo-benchmark for models of marine ice-sheet deglaciation*, Rev. Geophys. 53, pp. 1051–1098.  
50  
51  
52  
53  
54 588 Patton H., Hubbard A.L., Andreassen K., Auriac A., Whitehouse P.L., Stroeve A.P., Shackleton C.,  
55 Winsborrow M.C.M., Heyman J., Hall A.M., 2017, *Deglaciation of the Eurasian ice sheet complex*, Quaternary  
56 *Science Reviews*, Volume 169, ISSN 0277-3791, pp. 148 - 172.  
57  
58  
59  
60  
61  
62  
63  
64  
65

- 591 Peakall J., Kane A.I., Masson D.G., Keevil G., McCaffrey W., Corney R., 2012, *Global (latitudinal) variation*  
1  
2 592 *in submarine channel sinuosity*, *Geology* 40, pp. 11-14.  
3  
4  
5 593 Pedrosa M.T., Camerlenghi A., De Mol B., Urgeles R., Rebesco M., Lucchi R.G., 2011, *Seabed morphology*  
6  
7 594 *and shallow sedimentary structure of the Storfjorden and Kveithola trough-mouth fans (North West Barents*  
8  
9 595 *Sea)*, *Marine Geology*, 286, pp. 65-81.  
10  
11 596 Petrini M., Colleoni F., Kirchner N., Hughes A.L.C., Camerlenghi A., Rebesco M., Lucchi R.G., Forte E.,  
12  
13 597 Colucci R.R., Noormets R., 2018, *Interplay of grounding-line dynamics and sub-shelf melting during retreat of*  
14  
15 598 *the Bjørnøyrenna Ice Stream*, *Scientific Reports* 8, art. no. 7196.  
16  
17  
18 599 Pope E.L., Talling P.J., Ó Cofaigh C., 2018, *The relationship between ice sheets and submarine mass*  
19  
20 600 *movements in the Nordic Seas during the Quaternary*, *Earth-Science Reviews* 178, pp. 208-256.  
21  
22  
23 601 Rasmussen T., Thomsen E., Ślubowska A.M., Jessen S., Solheim A., Koc N. (2007). *Paleoceanographic*  
24  
25 602 *evolution of the SW Svalbard margin (76°N) since 20,000 14C yr BP*, *Quaternary Research - QUATERNARY*  
26  
27 603 *RES.* 67, pp. 100-114.  
28  
29  
30 604 Rebesco M., Liu Y., Camerlenghi A., Winsborrow M., Laberg J. S., Caburlotto A., Diviaco P., Accettella D.,  
31  
32 605 Sauli C., Wardell N., Tomini I., 2011, *Deglaciation of the western margin of the Barents Sea Ice Sheet — A*  
33  
34 606 *swath bathymetric and sub-bottom seismic study from the Kveithola Trough*, *Marine Geology*, 279, pp. 141-147.  
35  
36  
37 607 Rebesco M., Laberg J. S., Pedrosa M. T., Camerlenghi A., Lucchi R. G., Zgur F., Wardell N., 2014, *Onset and*  
38  
39 608 *growth of Trough-Mouth Fans on the North-Western Barents Sea margin — implications for the evolution of the*  
40  
41 609 *Barents Sea/Svalbard Ice Sheet*, *Quaternary Science Reviews* 92, pp. 227-234.  
42  
43  
44 610 Rebesco M., Özmaral A., Urgeles R., Accettella D., G. Lucchi R.G., Rütther D., Winsborrow M., Llopart J.,  
45  
46 611 Caburlotto A., Lantzsch H., Hanebuth T.J.J., 2016, *Evolution of a high-latitude sediment drift inside a*  
47  
48 612 *glacially-carved trough based on high-resolution seismic stratigraphy (Kveithola, NW Barents Sea)*, *Quaternary*  
49  
50 613 *Science Reviews* 147, pp. 178-193.  
51  
52  
53 614 Rise L., Bøe R., Riis F., Bellec V.K., Laberg J.S., Eidvin T., Elvenes S., Thorsnes T., 2013, *The Lofoten-*  
54  
55 615 *Vesterålen continental margin, North Norway: canyons and mass-movement activity*, *Mar. Pet. Geol.* 45, pp.  
56  
57 616 134–149.  
58  
59  
60  
61  
62  
63  
64  
65

- 1  
2 617 Robbins J.A., Edgington D.N., 1975. *Determination of recent sedimentation rates in Lake Michigan using Pb-*  
3  
4 618 *210 and Cs-137*. *Geochim. Cosmochim. Acta* 39, pp. 285–304.
- 5 619 Robbins J.A., Edgington D.N., Kemp A.L.W., 1978. *Comparative 210Pb, 137Cs, and pollen geochronologies of*  
6  
7 620 *sediments from Lakes Ontario and Erie*. *Quat. Res.* 10, pp. 256–278.
- 8  
9 621 Rütther D. C., Mattingsdal R., Andreassen K., Forwick M., Husum K., 2011, *Seismic architecture and*  
10  
11 622 *sedimentology of a major grounding zone system deposited by the Bjørnøyrenna Ice Stream during Late*  
12  
13 623 *Weichselian deglaciation*, *Quaternary Science Reviews* 30, pp. 2776–2792.
- 14  
15  
16 624 Rütther D. C., Bjarnadóttir L.R., Junttila J., Husum K., Rasmussen T.L., Lucchi R.G., Andreassen K., 2012,  
17  
18 625 *Pattern and timing of the northwestern Barents Sea Ice Sheet deglaciation and indications of episodic Holocene*  
19  
20 626 *deposition*, *Boreas*, pp. 1-19.
- 21  
22  
23 627 Rydningen T. A., Laberg J. S., & Kolstad V., 2015, *Seabed morphology and sedimentary processes on high-*  
24  
25 628 *gradient trough mouth fans offshore Troms, northern Norway*, *Geomorphology* 246, pp. 205-219.
- 26  
27  
28 629 Salvigsen O. and Slettemark ø., 1995, *Past glaciation and sea levels on Bjørnøya, Svalbard*, *Polar Research*, 14,  
29  
30 630 pp. 245–251.
- 31  
32  
33 631 Sanchez-Cabeza J.A., Ruiz-Fernández A.C., 2012. *210Pb sediment radiochronology: An integrated formulation*  
34  
35 632 *and classification of dating models*. *Geochim. Cosmochim. Acta* 82, pp. 183–200.
- 36  
37  
38 633 Shepard F.P., Emery K.O., 1941, *Submarine Topography off the California Coast: Canyons and Tectonic*  
39  
40 634 *Interpretations*, *Geological Society of America Special Paper* 31, 171 p.
- 41  
42  
43 635 Smith J.N., 2001. *Why should we believe 210Pb sediment geochronologies?* *J. Environ. Radioact.* 55, pp. 121–  
44  
45 636 123.
- 46  
47  
48 637 Stokes C.R., Clark C.D., 2001, *Paleo-ice streams*, *Quaternary Science Reviews*, Vol. 20, Issue 13, pp. 1437-  
49  
50 638 1457.
- 51  
52  
53 639 Vorren T.O., Lebesbye E., Andreassen K., Larsen K.B., 1989, *Glacigenic sediments on a passive continental*  
54  
55 640 *margin as exemplified by the Barents Sea*, *Mar. Geol.* 85, pp. 251-272.
- 56  
57  
58 641 Vorren T.O., Laberg J.S., 1996, *Late glacial air temperature, oceanographic and ice sheet interactions in the*  
59  
60 642 *southern Barents Sea region*, in: Andrews J.T., Austin W.E.N., Bergsten H., Jennings A.E. (Eds.), *Late*



- 643 *Quaternary Palaeoceanography of the North Atlantic Margins*, Special Publication No. 111, Geological  
1 Society, London, pp. 303-321.  
2  
3  
4  
5 645 Vorren T.O., Laberg J.S., Blaume F., Dowdeswell J. A., Kenyoh N.H., Mienert J., Rumohr J., Werner F., 1998,  
6  
7 646 *The Norwegian-Greenland sea continental margins: morphology and late quaternary sedimentary processes*  
8  
9 647 *and environment*, Quaternary Science Reviews, Vol. 17, pp. 273-302.  
10  
11 648 Vorren T.O., Laberg J.S., 2001, *Late Quaternary sedimentary processes and environment on the Norwegian-*  
12  
13 649 *Greenland Sea continental margins*, Sedimentary Environments Offshore Norway – Palaeozoic to Recent,  
14  
15 650 Norwegian Petroleum Society Special Publications, Elsevier, Vol. 10, pp. 451-456.  
16  
17  
18 651 Vorren T.O., Rydningen T.A., Baeten N.J., Laberg J.S., 2015, *Chronology and extent of the Lofoten-Vesterålen*  
19  
20 652 *sector of the Scandinavian Ice Sheet from 26 to 16 cal. Ka BP*, Boreas 44, pp. 445-458.  
21  
22  
23 653 Wang Y.Y., Zhan X.C., Yuan J.H., Fan X.T., 2011, *The evaluation of uncertainty in the results for elements*  
24  
25 654 *rubidium, strontium, yttrium and zirconium in silicate geological samples by polarized energy dispersive X-ray*  
26  
27 655 *fluorescence spectrometry*, Guang Pu Xue Yu Guang Pu Fen Xi, 31(6), pp. 1707-1711.  
28  
29  
30 656 Wilken M. and Mienert J., 2006, *Submarine glacigenic debris flows, deep-sea channels and past ice-stream*  
31  
32 657 *behaviour of the East Greenland continental margin*, Quat. Science Rev., pp. 784-810.  
33  
34  
35 658 Winsborrow M.C.M., Andreassen K., Corner G.D., Laberg J.S., 2010, *Deglaciation of a marine-based ice*  
36  
37 659 *sheet: Late Weichselian palaeo-ice dynamics and retreat in the southern Barents Sea reconstructed from*  
38  
39 660 *onshore and offshore glacial geomorphology*, Quat. Sci. Rev. 29, pp. 424-442.  
40  
41  
42 661 Wohlfarth B., Björck S., Possnert G., 1995, *The Swedish Time Scale — A potential calibration tool for the*  
43  
44 662 *radio-carbon time scale during the Late Weichselian*, Radio-carbon 37(2), pp. 347-60.  
45  
46  
47 663 Zecchin M., Rebesco M., Lucchi R.G., Caffau M., Lantzsich H., Hanebuth, T.J.J., 2016, *Buried iceberg-keel*  
48  
49 664 *scouring features in the southern Spitsbergenbanken, NW Barents Sea*, Marine Geology 382, pp. 68-79.  
50  
51  
52 665 Zecchin M., Rebesco M., 2018, *Glacigenic and glacial marine sedimentation from shelf to trough settings in the*  
53  
54 666 *NW Barents Sea*, Marine Geology 402, pp. 184-193.  
55  
56

57 **Captions:**  
58  
59  
60  
61  
62  
63  
64  
65

668 **Table 1** List of the multibeam systems used by name, acquisition year, cruise, research vessel, operating  
1  
2 669 frequency and beam number  
3

4  
5 670 **Fig. 1 a)** Map of the Arctic Ocean. The red square indicates the location of Fig. 1 b) Map of the NW Barents  
6  
7 671 Sea based on the International Bathymetric Chart of the Arctic Ocean (IBCAO) (*Jakobsson et al., 2012*). The  
8  
9 672 area of study is indicated by a yellow rectangle (Fig. 2). The dashed white line represents the extension of the  
10  
11 673 Svalbard-Barents-Kara Ice Sheet (SBKIS) during the Last Glacial Maximum (LGM) (*Hughes et al., 2016*)  
12

13  
14 674 **Fig. 2** Bathymetric map of the INBIS Channel System area. This map has been produced with all available  
15  
16 675 multibeam datasets, superimposed onto IBCAO (*Jakobsson et al., 2012*). The white dotted square marks the  
17  
18 676 inter-TMF area analysed in this paper (see Fig. 3a and 3b). Red lines highlight the major channels, while the  
19  
20 677 dashed red lines infer the maximum extension of the upper part area of the system. The dashed pink line  
21  
22 678 represents the INBIS Channel described by *Vorren et al. (1998)*. The Kveithola and Bear Island TMFs are  
23  
24 679 depicted by a yellow dashed line. Moraines, between 2 km and 5 km from the shelf edge, represent the outer  
25  
26 680 shelf limit of grounded slow-moving ice during the LGM (cf. Fig. 7c)  
27

28  
29 681 **Fig. 3** Slope gradient maps, uninterpreted (a) and interpreted (b) of the parts of INBIS Channel System analysed  
30  
31 682 in this paper (white dotted square in Fig. 2). The INBIS Channel System is divided into upper reaches (limited  
32  
33 683 by the dashed yellow line), northern and southern parts (separated by the dashed pink line). Bathymetric  
34  
35 684 sections in dip directions (A, C, E, G, I, K and M) and in strike directions (B, D, F, H, J, L and N) are depicted  
36  
37 685 in light blue. Six less visible channels are highlighted with dotted black lines. The main channel is highlighted  
38  
39 686 by a dashed red line. The location of cores HN17-06BC1, HN17-07BC2 and HN17-08BC3, collected during  
40  
41 687 High North 17 cruise, are depicted in green, purple and orange respectively  
42

43  
44 688 **Fig. 4** Photographs, X-radiographs, lithological logs together with graphs of wet bulk density, magnetic  
45  
46 689 susceptibility, Zr/Rb, Ca/Ti,  $^{210}\text{Pb}_{\text{xs}}$  and  $^{137}\text{Cs}$  of the two box cores recovered in the INBIS Channel System.  
47  
48 690 Core HN17-07BC2, in a gully on the continental slope, indicates fine-grained turbidites (terrigenous laminations  
49  
50 691 at the core bottom). Core HN17-08BC3, on the outer shelf, indicates the presence of a high-energy environment  
51  
52 692 with condensed sequences (lag deposit at the core top) unaffected by depositional gaps  
53

54  
55 693 **Fig. 5** Bathymetric sections in strike directions (B, D, F, H, J, L and N) of the INBIS Channel System. Location  
56  
57 694 in Fig. 3. Horizontal red dashed lines are to emphasise the relief of the levee deposits  
58

695 **Fig. 6** Bathymetric sections in dip directions (A, C, E, G, I, K and M) of the INBIS Channel System. Location in

1  
2 696 Fig. 3. Profile E (located inside the main channel) is twice as long; the orange dashed line indicates the same  
3  
4 697 point

5  
6  
7 698 **Fig. 7** Schemes of inferred pre-LGM state (a), LGM state (b) and post-LGM state (c) of the INBIS Channel

8  
9 699 System. Green arrows indicate the location and direction of area of fast-moving ice (ice streams, slightly darker

10  
11 700 than the rest of the ice sheet). Downslope, the gullies (thin black lines) merge and evolve into channels (thick

12  
13 701 black lines). Blue arrows (b) indicate the direction of glacial debris flows, forming depositional lobes on

14  
15 702 both Kveithola and Bear Island TMF (in yellow). During the ice sheet retreat (c) meltwaters (light blue) flow

16  
17 703 downslope past the shelf edge, both in the INBIS Channel System and in the Kveithola and Bear Island TMFs

18  
19 704 (in yellow). Meltwaters carve new gullies into the glacial debris flow deposits in the southern part of the

20  
21 705 INBIS Channel System (pink area) and on the TMFs (see Fig. 7b for comparison). Shelf-edge moraines

22  
23 706 (labelled in grey) mark the maximum extent of the ice sheet around Bear Island

Name	Acquisition year	Cruise(s)	Research Vessels	Operating Frequency	Beam number
MB8111	2008/2015	EGLACOM / DEGLABAR	OGS Explora	100 kHz	101
MB8150	2008	EGLACOM	OGS Explora	12 kHz	234
MB7150	2015	DEGLABAR	OGS Explora	12 kHz	880
EM1002	2013	CORIBAR	Maria S. Merian	95 kHz	111
EM122	2013	CORIBAR	Maria S. Merian	12 kHz	432
EM302	2017	High North 17	NRV Alliance	30 kHz	864

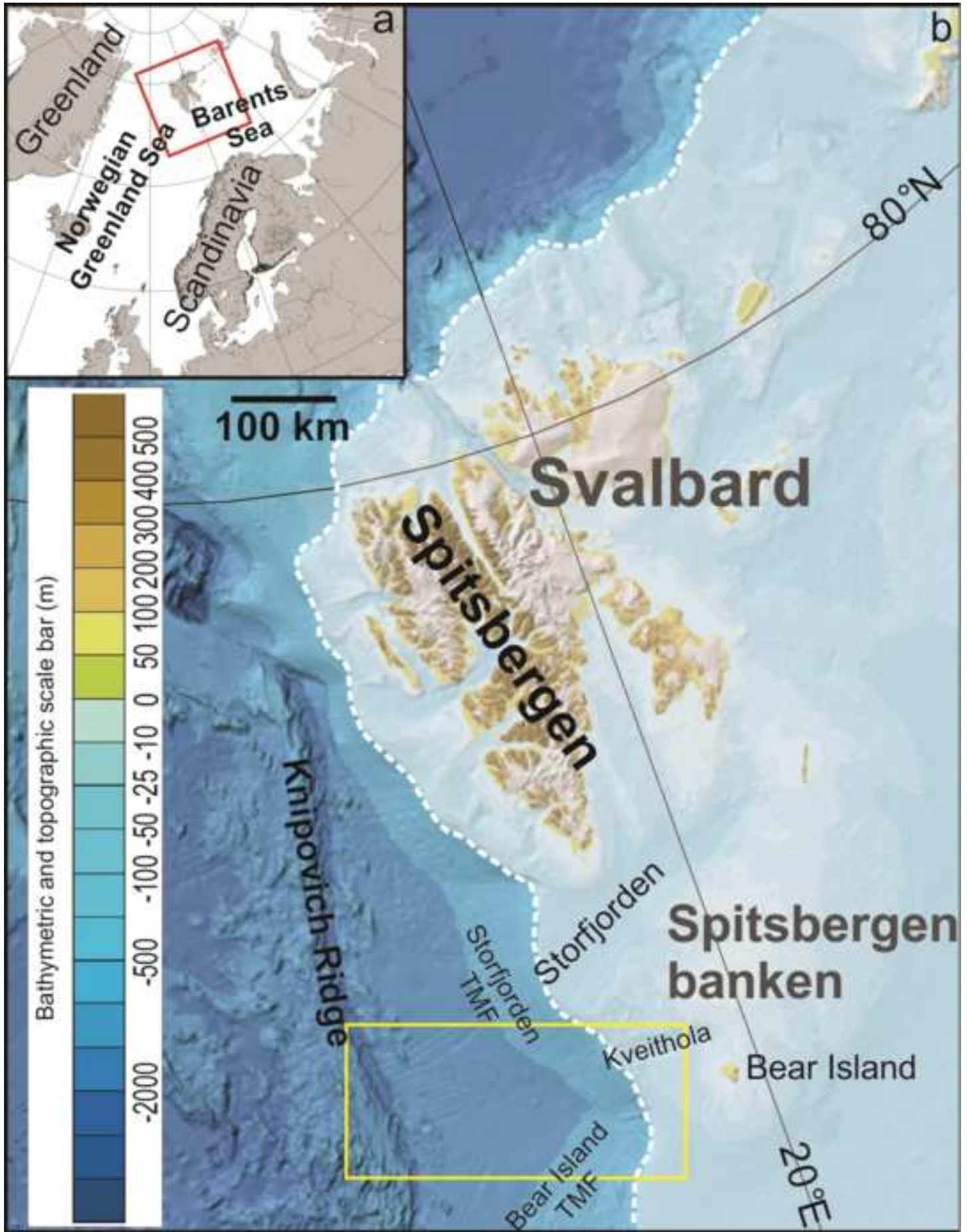


Figure 2

